SPhT-T07/026
RBRC-647

Exclusive vector meson production at HERA from QCD with saturation

C. Marquet*
RIKEN BNL Research Center, Brookhaven National Laboratory, Upton, NY 11973, USA

R. Peschanski†
Service de Physique Théorique, CEA/Saclay, 91191 Gif-sur-Yvette cedex, France
URA 2306, unité de recherche associée au CNRS

G. Soyez‡§
LPTHE, Université P. et M. Curie (Paris 6), Université D. Diderot (Paris 7)
Tour 24-25, 5e Etage, Boîte 126, 4 place Jussieu, 75252 Paris cedex 05, France
UMR 7589, unité mixte de recherche du CNRS

Following recent predictions that the geometric scaling properties of deep inelastic scattering data in inclusive $\gamma^* p$ collisions are expected also in exclusive diffractive processes, we investigate the diffractive production of vector mesons. Using analytic results in the framework of the BK equation at non-zero momentum transfer, we extend to the non-forward amplitude a QCD-inspired forward saturation model including charm, following the theoretical predictions for the momentum transfer dependence of the saturation scale. We obtain a good fit to the available HERA data and make predictions for deeply virtual Compton scattering measurements.

I. INTRODUCTION

Geometric scaling [1] is a striking feature of deep inelastic scattering (DIS) data at small Bjorken x, or at large rapidity $Y = \log(1/x)$. The photon-proton total cross section $\sigma_{\rm tot}^{\gamma^* p\to X}(x, Q^2)$ obeys a scaling in the single variable $Q^2/Q_s^2(x)$ where Q is the virtuality of the photon and Q_s the *saturation scale*. This momentum scale increases with rapidity according to $Q_s^2(x) = Q_0^2\, x^{-\lambda}$ with $\lambda \sim 0.3$ and $Q_0 \sim 0.1$ GeV (giving a saturation scale of order 1 GeV for $x \sim 10^{-4}$). Recently, the diffractive cross-section $\sigma_{\rm diff}^{\gamma^* p\to Xp}$ and the elastic vector-meson production cross-section $\sigma_{\rm VM}^{\gamma^* p\to Vp}$ were shown to also feature scaling behaviours, with the same saturation scale [2].

From the theoretical point of view, the high-energy or small$-x$ limit can be studied within the QCD dipole picture [3]. Introducing the dipole-proton elastic scattering amplitude $T(r, Y)$, where r is the transverse size of the dipole, the corresponding law $T(r, Y) = T(rQ_s(Y))$ appears to be a genuine consequence of saturation effects [4] characteristic of the high-density regime of perturbative QCD. More precisely, the evolution towards saturation is conveniently described by the non-linear Balitsky-Kovchegov (BK) equation [5] that resums QCD fan diagrams in the leading-logarithmic approximation. Geometric scaling for $T(r, Y)$ appears to be a mathematical consequence of the asymptotic solution in Y of this nonlinear equation in terms of travelling waves [6]. Within this theoretical framework, $Q_s(Y) = Q_0\Omega_s(Y)$ and the rapidity dependence of the saturation scale, given by $\Omega_s(Y)$, is then obtained from features of the Balitsky-Fadin-Kuraev-Lipatov [7] (BFKL) kernel, which drives the linear regime of the BK evolution.

The total cross section $\sigma_{\rm tot}^{\gamma^* p\to X}$ (as well as the diffractive cross section $\sigma_{\rm diff}^{\gamma^* p\to Xp}$ and the elastic vector-meson production cross section $\sigma_{\rm VM}^{\gamma^* p\to Vp}$) is related to the forward elastic dipole-proton amplitude. It is natural to ask the question whether geometric scaling survives when considering non-forward amplitudes. To that purpose, it is temptative to study the BK equation which is written for $T(\mathbf{r}, \mathbf{b}; x)$, the dipole-proton elastic scattering amplitude, depending not only on the dipole size $\mathbf{r}$ but also on the impact parameter $\mathbf{b}$. However, the aforementioned scaling law cannot be easily adapted to account for the impact parameter dependence. The analysis of the BK equation in impact-parameter space [8, 9] even shows a contradiction with confinement: the large-$\mathbf{b}$ dependence of the solutions develops a power-law tail with decreasing x.

Previous studies [10, 11] have shown that the travelling-wave method can be extended to the BK equation with transverse-space kinematical dependence provided one investigates the problem in terms of momentum transfer instead

‡ on leave from the fundamental theoretical physics group of the University of Liège.
*Electronic address: marquet@quark.phy.bnl.gov
†Electronic address: pesch@spht.saclay.cea.fr
§Electronic address: g.soyez@ulg.ac.be

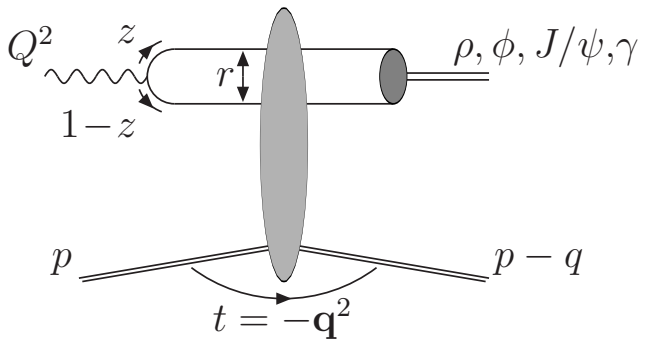

FIG. 1: Vector-particle production in the dipole frame. The amplitude factorises as a product of vertex functions and elastic dipole-proton interaction amplitude (see formula (3)).

of impact parameter. The remarkable point [10] is that the travelling-wave analysis of the BK equation can be better achieved in momentum space, by Fourier transforming $T(\mathbf{r},\mathbf{b};Y)$ into $\tilde{T}(\mathbf{r},\mathbf{q};Y)$ where $\mathbf{q}$ is the momentum transfer. From the knowledge of the exact solutions of the BFKL equation at non-zero momentum transfer [12], the travelling-wave property has been extended [10] (for large Q):

- at small momentum transfer, *i.e.* when $|\mathbf{r}||\mathbf{q}| < |\mathbf{r}|Q_0 < |\mathbf{r}|Q \sim 1$, one has asymptotically $\tilde{T}(\mathbf{r},\mathbf{q};Y) = \tilde{T}(|\mathbf{r}|Q_0\Omega_s(Y),\mathbf{q})$, recovering the forward result;
- at intermediate, semi-hard, momentum transfer, *i.e.* when $|\mathbf{r}|Q_0 < |\mathbf{r}||\mathbf{q}| < |\mathbf{r}|Q \sim 1$, one has asymptotically $\tilde{T}(\mathbf{r},\mathbf{q};Y) = \tilde{T}(|\mathbf{r}||\mathbf{q}|\Omega_s(Y),\mathbf{q})$;
- at large, hard, momentum transfer, *i.e.* when $|\mathbf{r}|Q_0 < |\mathbf{r}|Q < |\mathbf{r}||\mathbf{q}| \sim 1$, one has no more saturation, (giving an explanation of the impact-parameter puzzle).

This introduces a $\mathbf{q}$-dependent saturation momentum in the near-forward and intermediate transfer region with a rapidity evolution $\Omega_s(Y)$ keeping the same form as in the forward case. Those predictions were confirmed both by analytical and numerical analysis of the BK equation completely formulated in momentum space [11].

Our purpose here is to investigate an interesting phenomenological prediction from these results: the geometric scaling property should manifest itself in exclusive vector meson production and deeply virtual Compton scattering (DVCS), which are experimentally measured at moderate non-zero momentum transfer $t = -\mathbf{q}^2$. In this paper, we analyse whether or not the available data from HERA are sensitive to a $t-$dependent saturation scale. To do this, we use a QCD-inspired saturation model for the dipole amplitude $\tilde{T}(\mathbf{r},\mathbf{q};Y)$. Since it is important to include the charm in the analysis, both for its impact on DVCS, non-charmed mesons and also J/Ψ production, we make use of a recent saturation model that successfully includes charm [13]. Note that our parametrisation, which uses the momentum transfer $\mathbf{q}$ instead of the impact parameter $\mathbf{b}$ as suggested by this derivation of saturation effects in perturbative QCD, provides a fruitful phenomenological framework since the data are directly measured as a function of $t = -\mathbf{q}^2$.

The plan of the paper is as follows. In section II, we recall the formulation of vector meson production and DVCS differential cross-sections in terms of the dipole scattering amplitude $\tilde{T}(\mathbf{r},\mathbf{q};x)$. In section III, we briefly explain the asymptotic travelling-wave properties of this amplitude and how they translate into geometric scaling at non zero momentum transfer; we also introduce our QCD-inspired model for $\tilde{T}$. In Section IV, we present fits to the vector-meson production experimental data, discuss our results and present predictions for DVCS. Section V concludes.

II. EXCLUSIVE VECTOR MESON PRODUCTION IN DIS AT SMALL x

In the small$-x$ limit, it is convenient to describe the scattering of the photon in a particular frame, called the *dipole frame*, in which the virtual photon undergoes the hadronic interaction via a fluctuation into a colorless $q\bar{q}$ pair, called dipole, which then interacts with the target proton. The wavefunctions $\psi^{\gamma^*,\lambda}_{f,h,\bar{h}}(z,\mathbf{r};Q^2)$ describing the splitting of a virtual photon with polarization $\lambda = 0,\pm 1$ into a dipole are well known. The indices $h = \pm 1$ and $\bar{h} = \pm 1$ denote the helicities of the quark and the antiquark composing the dipole of flavor f. The wavefunctions depend on the virtuality Q^2, the fraction z of longitudinal momentum (with respect to the $\gamma^* - p$ collision axis) carried by the quark, and the two-dimensional vector $\mathbf{r}$ whose modulus is the transverse size of the dipole. Explicit formulæ for the QED functions $\psi^{\gamma^*,\lambda}_{f,h,\bar{h}}$ can be found in the literature [14] and are recalled in Appendix A.

The exclusive production of vector mesons is represented in Fig.1: the photon splits into a dipole of size $\mathbf{r}$ which scatters elastically off the proton, with momentum transfer $\mathbf{q}$, and recombines into a vector meson whose mass we shall denote M_V. To describe this process, we need to introduce the wavefunctions $\psi^{V,\lambda}_{f,h,\bar{h}}(z,\mathbf{r};M_V^2)$ which describe the splitting of the vector meson with polarization λ into the dipole. In fact, to compute the vector-meson production amplitude pictured in Fig.1, we need the transverse (T) and longitudinal (L) *overlap functions* $\Phi_T^{\gamma^* V}=(\Phi_+^{\gamma^* V}+\Phi_-^{\gamma^* V})/2$ and $\Phi_L^{\gamma^* V}=\Phi_0^{\gamma^* V}$ obtained through

$$\Phi_\lambda^{\gamma^* V}(z,\mathbf{r};Q^2,M_V^2)=\sum_{fh\bar{h}}\left[\psi^{V,\lambda}_{f,h,\bar{h}}(z,\mathbf{r};M_V^2)\right]^*\psi^{\gamma^*,\lambda}_{f,h,\bar{h}}(z,\mathbf{r};Q^2)\ . \tag{1}$$

These functions depend on the meson wavefunctions $\psi^{V,\lambda}_{f,h,\bar{h}}$, and different models exist in the literature [15, 16, 17]. We shall discuss two different choices later in this paper: the *boosted Gaussian* (BG) wavefunctions [15] and the *light-cone Gaussian* (LCG) wavefunctions [17]. For completeness, we give explicit expressions for those overlap functions in Appendix A.

If $\mathbf{q}$ denotes the transverse momentum transfered by the proton during the collision, the differential cross-section with respect to $t=-\mathbf{q}^2$ reads

$$\frac{d\sigma^{\gamma^* p\to Vp}_{T,L}}{dt}=\frac{1}{16\pi}\left[1+(\beta^{(V)}_{T,L})^2\right]\left|\mathcal{A}^{\gamma^* p\to Vp}_{T,L}\right|^2. \tag{2}$$

In that expression, $\mathcal{A}$ refers to the imaginary part of the scattering amplitude and is given by

$$\mathcal{A}^{\gamma^* p\to Vp}_{T,L}=\int d^2x\,d^2y\int_0^1 dz\ \Phi^{\gamma^* V}_{T,L}(z,\mathbf{x}-\mathbf{y};Q^2,M_V^2)\ e^{i\mathbf{q}\cdot\mathbf{y}}\ T(\mathbf{x},\mathbf{y};Y)\ , \tag{3}$$

where $\mathbf{x}$ and $\mathbf{y}$ are respectively the transverse positions of the quark and the antiquark forming the dipole. $T(\mathbf{x},\mathbf{y};Y)$ is the dipole-proton scattering amplitude and carries all the energy dependence via the rapidity Y which is now obtained from the centre-of-mass energy W and the vector-meson mass M_V using

$$Y=\log\left(\frac{W^2+Q^2}{M_V^2+Q^2}\right)\ .$$

The prefactor $1+\beta^2$ in (2) accounts for the contribution coming from the real part of the amplitude and can be obtained using dispersion relations:

$$\beta^{(V)}_{T,L}=\tan\left(\frac{\pi\lambda}{2}\right)\qquad\text{with}\qquad\lambda=\frac{\partial\log(\mathcal{A}^{\gamma^* p\to Vp}_{T,L})}{\partial\ \log(1/x)}\ . \tag{4}$$

It is convenient to consider the dipole-proton scattering amplitude as a function of $\mathbf{r}=\mathbf{x}-\mathbf{y}$ and $\mathbf{b}=z\mathbf{x}+(1-z)\mathbf{y}$ and to introduce the following Fourier transform:

$$\tilde{T}(\mathbf{r},\mathbf{q};Y)=\int d^2b\ e^{i\mathbf{q}\cdot\mathbf{b}}\ T(\mathbf{r},\mathbf{b};Y)\ . \tag{5}$$

Indeed, as we shall discuss in the next section, this quantity features the geometric scaling property at non-zero momentum transfer. The formula we shall use finally reads

$$\frac{d\sigma^{\gamma^* p\to Vp}_{T,L}}{dt}=\frac{1}{16\pi}\left[1+(\beta^{(V)}_{T,L})^2\right]\left|\int d^2r\int_0^1 dz\ \Phi^{\gamma^* V}_{T,L}(z,\mathbf{r};Q^2,M_V^2)\ e^{-iz\mathbf{q}\cdot\mathbf{r}}\ \tilde{T}(\mathbf{r},\mathbf{q};Y)\right|^2\ . \tag{6}$$

Note that formula (6) can also be used to compute the DVCS cross-section $\sigma^{\gamma^* p\to\gamma p}$, provided one uses the vertex for a real photon instead of a vector meson in (1). The overlap function between the incoming virtual photon and the outgoing transversely-polarized real photon is now model-independent and given by

$$\Phi_T^{\gamma^*\gamma}(z,\mathbf{r};Q^2)=\sum_{fh\bar{h}}\left[\psi^{\gamma^*,T}_{f,h,\bar{h}}(z,\mathbf{r};0)\right]^*\psi^{\gamma^*,T}_{f,h,\bar{h}}(z,\mathbf{r};Q^2)\ . \tag{7}$$

III. GEOMETRIC SCALING AT NON-ZERO MOMENTUM TRANSFER

We have expressed the exclusive vector-meson production cross-sections (6) in the high-energy limit in terms of the Fourier-transformed dipole scattering amplitude off the proton $\tilde{T}(\mathbf{r},\mathbf{q};Y)$. Its evolution towards large values of Y is computable from perturbative QCD and the most important result about the growth of the dipole amplitude towards the saturation regime is probably the geometric scaling regime. It first appeared in the context of the proton structure function, which involves the dipole scattering amplitude at zero momentum transfer. At small values of x, instead of being a function of *a priori* the two variables $r=|\mathbf{r}|$ and Y, the dipole scattering amplitude is actually a function of the single variable $r^2Q_s^2(Y)$ up to inverse dipole sizes significantly larger than the saturation scale $Q_s(Y)$. More precisely, one can write

$$\tilde{T}(\mathbf{r},\mathbf{q}=0;Y) = 2\pi R_p^2\, N(r^2Q_s^2(Y))\ , \tag{8}$$

implying (for massless quarks) the geometric scaling of the total cross-section at small x : $\sigma_{\rm tot}^{\gamma^* p\to X}(Y,Q^2) = \sigma_{\rm tot}^{\gamma^* p\to X}(\tau=Q^2/Q_s^2(Y))$. This has been confirmed by experimental data [1] (see also [2] for the geometric scaling of the diffractive and elastic vector-meson production cross-sections) with $Q_s^2(Y) = Q_0^2 e^{\lambda Y}$, and the parameters $\lambda\sim 0.3$ and $Q_0\sim 0.1$ GeV.

As explained in the Introduction, it has been shown in a recent work [10, 11] that the geometric scaling property can be extended to the case of non zero momentum transfer, provided $r|\mathbf{q}|\ll 1$. We obtained that equation (8) can be generalised to

$$\tilde{T}(\mathbf{r},\mathbf{q};Y) = 2\pi R_p^2\, f(\mathbf{q})\, N(\mathbf{r}^2Q_s^2(Y,\mathbf{q}))\ , \tag{9}$$

with the asymptotic behaviours $Q_s^2(Y,\mathbf{q}) \sim \max(Q_0^2,\mathbf{q}^2)\exp(\lambda Y)$ and an unknown form factor $f(\mathbf{q})$ of non-perturbative origin.

In practice, we need to specify three ingredients:

- The $\mathbf{q}$ dependence of the saturation momentum is parametrised as

$$Q_s^2(Y,\mathbf{q}) = Q_0^2(1+c\mathbf{q}^2)\, e^{\lambda Y} \tag{10}$$

  in order to interpolate smoothly between the small and intermediate transfer regions.

- The form factor $f(\mathbf{q})$ catches the transfer dependence of the proton vertex. It has to be noticed that this form factor is factorised from the projectile vertices and thus does not spoil the geometric scaling properties. For simplicity, we use $f(\mathbf{q}) = \exp(-B\mathbf{q}^2)$.

- The scaling function N is obtained from the forward saturation model [13, 18]:

$$N(rQ_s(Y),Y) = \begin{cases} N_0\left(\frac{r^2Q_s^2(Y)}{4}\right)^{\gamma_c}\ \exp\left[-\frac{\ln^2(r^2Q_s^2(Y)/4)}{2\kappa\lambda Y}\right] & \text{for } r^2Q_s^2(Y)\le 4 \\ 1-e^{-\alpha\ln^2(\beta\mathbf{r}^2Q_s^2(Y))} & \text{for } r^2Q_s^2(Y)>4 \end{cases} \tag{11}$$

  with α and β uniquely determined from the conditions that N and its derivative are continuous at $r^2Q_s^2(x)=4$. The amplitude at the matching point is chosen to be $N_0=0.7$.

  In this work, we shall consider the same form for the forward amplitude as in the Iancu-Itakura-Munier (IIM) saturation model [18] but in its version extended in [13] to include heavy quarks (with $m_c=1.4$ GeV, $m_b=4.5$ GeV, and $m_f=0.14$ GeV for the light flavors). The coefficient $\kappa=9.9$ is obtained from the BFKL kernel while the critical exponent $\gamma_c=0.7376$ is fitted to the HERA measurements of the proton structure function, along with the remaining parameters. The saturation scale parameters are $\lambda=0.2197$ and $Q_0=0.298$ GeV and the proton radius is $R_p=3.34$ GeV^{-1}. Note that, after including heavy quark contributions, the saturation scale stays above 1 GeV for $x=10^{-5}$, rather than dropping to about 500 MeV as is the case in other studies (see the discussion in [13]). This parametrization is also successful in describing inclusive diffraction data [19].

  The last factor in the expression for small dipole sizes introduces geometric scaling violations, important when Y is not large enough, as predicted by the high-energy QCD evolution. It controls the way how geometric scaling is approached. Indeed, it can be neglected for $\log(r^2Q_s^2/4) < \sqrt{2\kappa\lambda Y}$, meaning that the geometric scaling window extends like $\sqrt{Y}$ above the saturation scale (in logarithmic units).

The final expression of our QCD-based saturation model is thus

$$\tilde{T}(\mathbf{r},\mathbf{q};x) = 2\pi R_p^2\, e^{-B\mathbf{q}^2} N(\mathbf{r}Q_s(x,\mathbf{q}),Y) \tag{12}$$

which is an extension of the forward model [13, 18] including the QCD predictions for non zero momentum transfer. Indeed, this model reproduces the initial model for q = 0 and ensures that the saturation scale has the correct asymptotic behaviours. We have two parameters: c related to the scale at which the q−dependence of the saturation scale becomes important and B, the t−slope of the form factor that we have taken as simple as possible. Those parameters have to be fitted to the experimental measurements of elastic vector-meson production as we shall comment in details in the next section.

Note that the form factor depends on a single slope B, independently of the vector-meson in the final state. This is in agreement with predictions from the BK equation [10, 11] which implies the factorisation of the non-perturbative contribution in (12). The difference in the processes of ρ, ϕ and J/Ψ production (or even DVCS cross-sections) fully comes from the vector-meson wavefunctions. Through their wavefunction, different vector mesons are sensitive to different dipole sizes, and thus feel saturation differently.

IV. FIT RESULTS AND DISCUSSION

In this section, we compare our formulation (6) and (12) for vector-meson production with the experimental measurements of ρ, ϕ and J/Ψ elastic production. We shall first state explicitly the data used to perform the fit, then give more details concerning the fit itself, present our results and compare them with other possible approaches, and finally we shall give predictions for DVCS measurements.

A. Data selection

In this analysis, we shall include the differential cross-section $d\sigma/dt$ as well as the elastic cross-section $\sigma_{\rm el}$. The dataset is obtained from the ρ-meson production measured by H1 [20], the ϕ-meson production measured by ZEUS [21], and the J/Ψ-meson production measured by ZEUS [22] and H1 [23]. We have not taken into account the ZEUS data for ρ mesons [24] since they lie in the low-Q^2 region where we do not expect the condition $r|q| \sim \sqrt{|t|/Q^2} \ll 1$ to be valid. The ratio $R = \sigma_L/\sigma_T$ between the longitudinal and transverse elastic cross-sections is mostly dependent of the choice of wavefunction, hence we have not included it in the analysis. Finally, this gives a total of 269 data points which have to be reproduced with the two parameters B and c in equation (12). Indeed, we keep the same parameters as in [13] for $t = 0$ as they provide a good description of the inclusive F_2 data.

B. Meson wavefunctions and alternative models

In order to test the quality of our parametrisation with t−dependent saturation scale, we shall compare our results with two alternative parametrisations. Since the main aim of this work is to analyse the t−dependence of the saturation scale, the first alternative we shall consider is a model in which we only adjust the slope B while keeping the saturation scale independent of the momentum transfer.

For the second alternative, we notice that if one assumes a slope B for the differential cross-sections at a given W and Q^2, the slope is experimentally observed to depend on Q^2. Within our parametrisation, it is the t dependence of the saturation scale which is expected to account for this behaviour in Q^2. This will be compared with a model where we keep Q_s constant in t ($c = 0$) and explicitly introduce a Q^2 dependence of the slope B. We shall use $B(Q^2) = B + B'/(Q^2 + M_V^2)$, which shows the same trend as the experimental estimations of $B(Q^2)$. Note however that this last two-parameter model is not compatible with the factorisation formula (6), valid at small values of x, where only the wavefunctions depend explicitly on Q^2.

Moreover, in order to understand to what extend our analysis depends upon the model used for the vector-meson wavefunctions, we shall test the dependence of our results with respect to two choices which have already proven to give good results. As mentioned before, we will consider the boosted Gaussian (BG) and the light-cone Gaussian (LCG) wavefunctions. For completion of the phenomenological discussion, we will also introduce some other combinations of wave-functions called BLL and BLB, as explained in the next subsection.

VM	Observable	N_{pts}	χ^2/N_{pts} for t-dependent Q_s				t-independent Q_s for BLB case	
			BG	LCG	BLL	BLB	B = constant	$B(Q^2+M_V^2)$
ρ	$\sigma_{\rm el}$	47	0.984	1.486	0.888	0.936	1.182	1.745
	$\frac{d\sigma}{dt}$	50	1.517	1.861	1.654	1.576	2.375	1.572
ϕ	$\sigma_{\rm el}$	34	1.999	1.304	1.323	1.327	2.732	1.175
	$\frac{d\sigma}{dt}$	70	1.452	1.115	1.049	0.978	1.321	0.746
J/Ψ	$\sigma_{\rm el}$	44	0.747	0.492	0.587	0.655	2.398	0.936
	$\frac{d\sigma}{dt}$	24	2.315	2.336	2.286	2.239	2.534	2.266
	Total	269	1.412	1.349	1.203	**1.186**	1.955	1.295

TABLE I: χ^2 results of the fits to the vector-meson production data. The different wavefunctions indicated (BG, LCG, BLL, BLB) are discussed in the text. For the best wavefunction (BLB), the χ^2 values are compared with alternative models, that feature a $t-$independent saturation scale.

Parameter	t-dependent Q_s				t-independent Q_s (BLB)	
	BG	LCG	BLL	BLB	B=const.	$B(Q^2+M_V^2)$
c (GeV^{-2})	4.077 ± 0.310	4.472 ± 0.325	4.258 ± 0.332	4.041 ± 0.311	-	-
B (GeV^{-2})	3.754 ± 0.095	3.724 ± 0.093	3.708 ± 0.097	3.713 ± 0.096	2.011 ± 0.031	1.447 ± 0.043
B'	-	-	-	-	-	4.245 ± 0.325

TABLE II: Parameters obtained from the fits. The parameters of our model do not vary much when using different wavefunctions. The LCG wavefunction describes better the ϕ meson and the BG wavefunction describes better the ρ meson. This is why the BLL or BLB choices give better global descriptions.

C. Results

We show in Table I the χ^2 corresponding to the fits of the different models presented above to the specified data. The parameters associated with those fits are given in Table II. In both tables, successive columns show the results for our model with $t-$dependent saturation scale convoluted with BG, LCG, BLL and BLB wavefunctions (we shall discuss the wavefunctions labelled BLL and BLB in a moment), followed by the two alternative models without momentum-transfer-dependence in the saturation scale (using BLB wavefunction). Those results show that our approach gives good results for vector-meson production and this is confirmed by Figures 2 and 3 on which we have plotted the curves for our fit together with the experimental data points.

It can be realized from Figs.2 and 3 that we obtain a satisfactory description of all data, considering the very small number of free parameters. It is of particular relevance for the inclusion of charm in the analysis to obverve that the different behaviour of the J/Ψ cross-section at fixed W from lighter vector mesons is reproduced within the same model. Hence the predicted mass dependence (via the rapidity dependence) together with the transfer dependence of the saturation scale seem to be both relevant in the successful description of data. Indeed, in our parametrisation, the mass dependence is not present in the non perturbative form factor.

Some technical comments are in order:

- First we notice that the J/Ψ differential cross-section always features a bad χ^2, and this is the case for all the wavefunctions and models studied. This is probably due to a normalization discrepancy between the H1 and ZEUS data, which are both included in the fit (in all the cases under consideration, we obtain a good description of the ZEUS data and a rather poor description of the H1 data) . Fortunately, this concerns only a few points, and it does not alter the global χ^2 too much.

- We obtain decent fits with both the BG and LCG wavefunctions though, if we have a closer look at the partial values of χ^2, we realise that there is a significant dependence on the choice for the wavefunction. The LCG description is significantly better for the ϕ meson while the BG description is better in the ρ meson case. Globally, the LCG χ^2 is slightly better than the BG one.

  This inspired the following studies: using simultameously the LCG wavefunction for the ϕ meson and the BG wavefunction for the ρ meson. When the LCG wavefunction is used for the J/Ψ the analysis is labeled BLL, and when the BG one is used, it is called BLB.

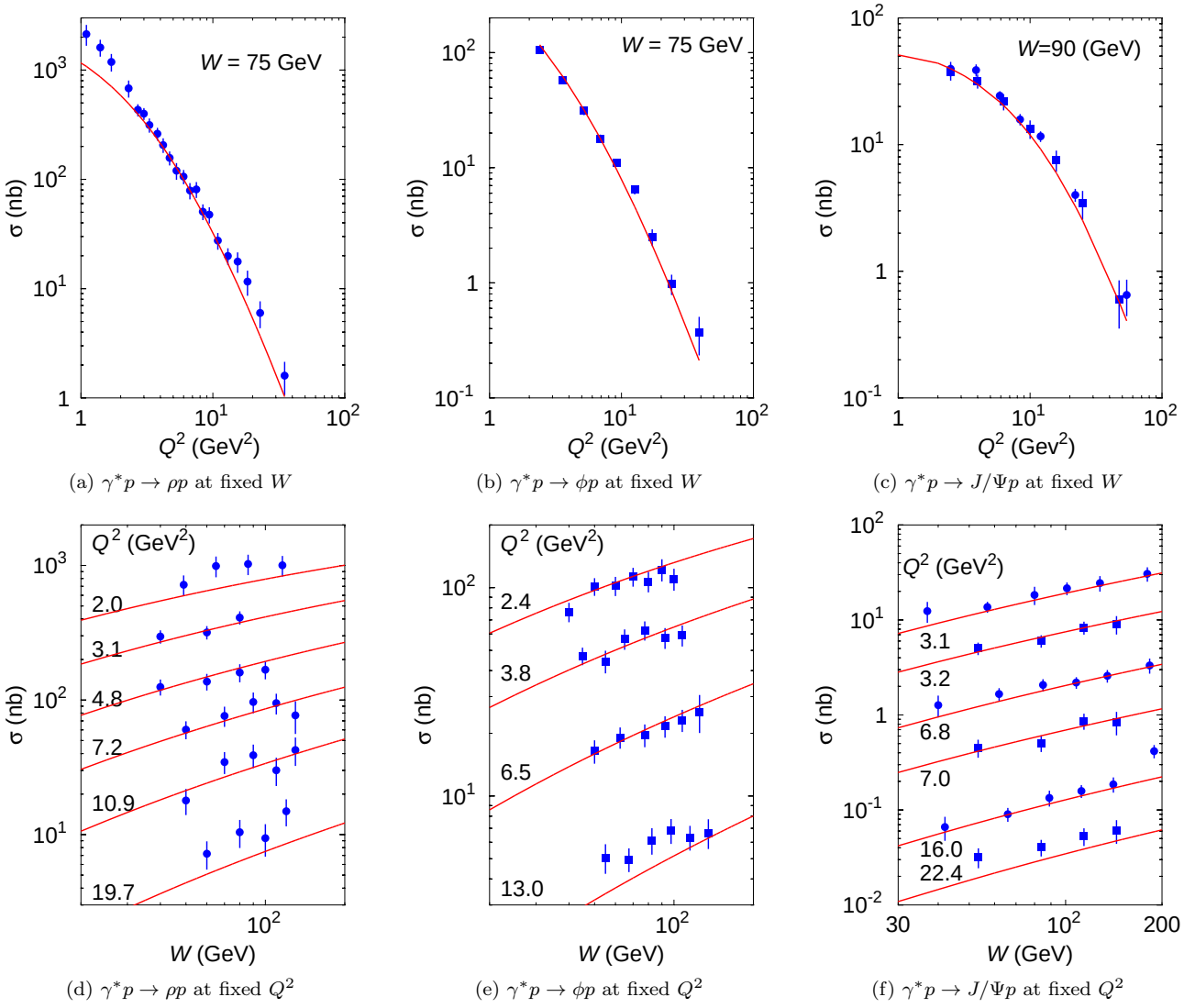

(a) $\gamma^* p \to \rho p$ at fixed W (b) $\gamma^* p \to \phi p$ at fixed W (c) $\gamma^* p \to J/\Psi p$ at fixed W

(d) $\gamma^* p \to \rho p$ at fixed Q^2 (e) $\gamma^* p \to \phi p$ at fixed Q^2 (f) $\gamma^* p \to J/\Psi p$ at fixed Q^2

FIG. 2: Fit results for the ρ (H1 [20]), ϕ (ZEUS [21]) and J/Ψ (ZEUS [22]) elastic cross-sections.

One sees that these combinations really improve the χ^2 values (this is the case for all the three models under study). In addition, the parameters c and B do not depend much on the choice of the wavefunction. Hence, this represents a good global description of the data and shows that the confrontation of our model with the experiments is successful.

- Comparing fits performed with our parametrisation (12) and the corresponding one with a $t-$*independent* saturation scale and constant slope, one sees that the introduction of $Q_s(t)$ significantly improves the fit. This significative result, which is consistent with theoretical expectations, opens the way for further experimental test of the saturation regime of QCD with exclusive processes.

  Compared to our prametrisation, the parametrisation with a $t-$*independent* saturation scale and with $B(Q^2) = B + B'/(Q^2 + M_V^2)$ shows χ^2 values lower in the ϕ-meson case but higher in the ρ- and J/Ψ-meson case. The global χ^2 is slightly higher than that of our QCD-inspired model, in which this effective behaviour in Q^2 is accounted for by t dependence of the saturation scale.

  In all cases, we have used the BLB choice for the wavefunctions as it gives the best results. By doing this we hope to minimise the impact of the wavefunctions in our discussion and focus on the description of the t dependence of the scattering amplitude.

  For better comparison with the other parametrisations, we have displayed in Figure 4 the curves corresponding

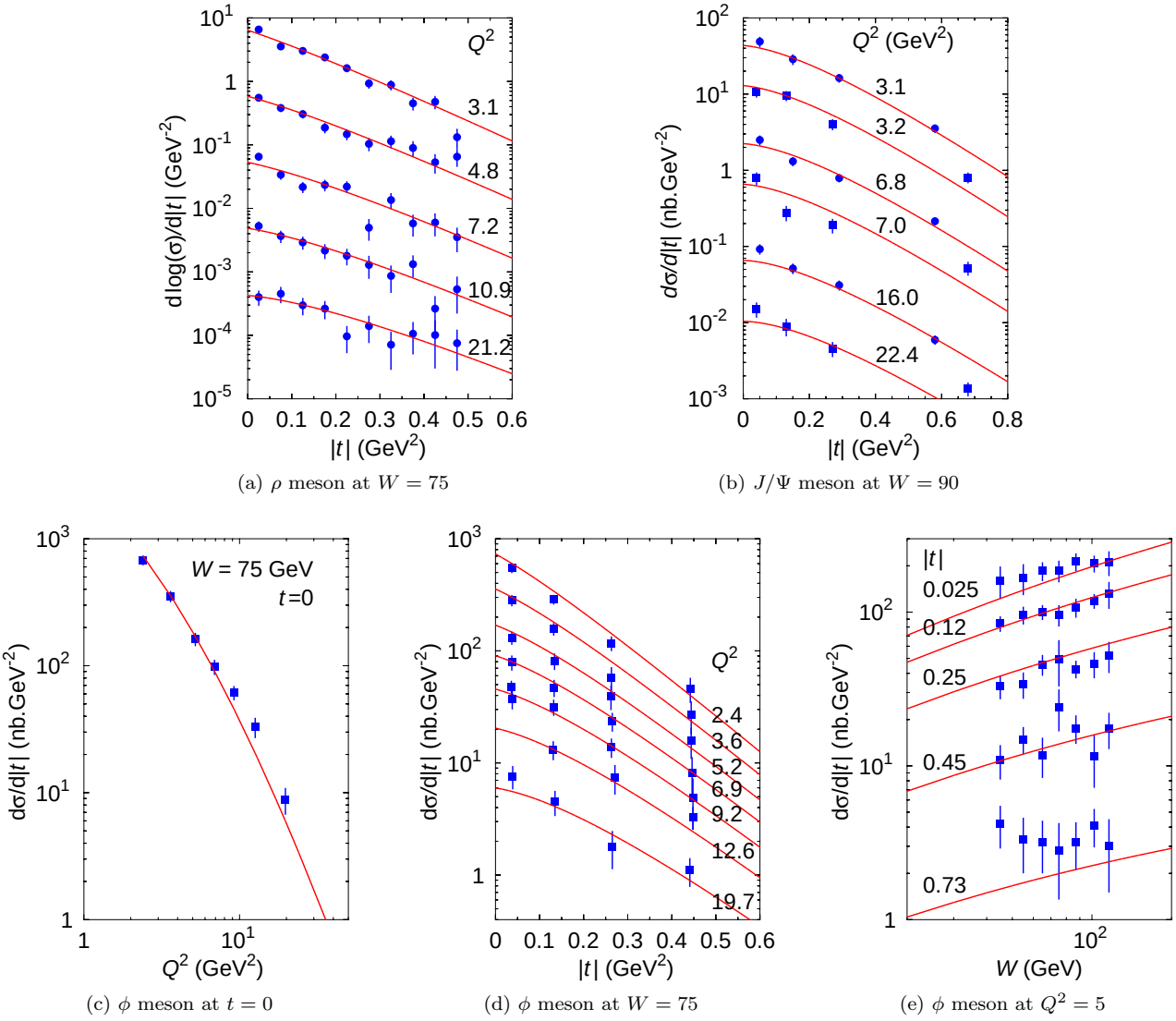

(a) ρ meson at $W = 75$

(b) J/Ψ meson at $W = 90$

(c) ϕ meson at $t = 0$

(d) ϕ meson at $W = 75$

(e) ϕ meson at $Q^2 = 5$

FIG. 3: Fit results for the ρ (H1 [20]), ϕ (ZEUS [21]) and J/Ψ (ZEUS [22], H1 [23]) differential cross-section.

to the three parametrisations of Table I (our t-dependent parametrisation for the BLB wavefunctions together with the two t-independent ones) for ρ-, ϕ- and J/Ψ-meson differential cross-sections for the lower and higher available values of Q^2.

- The plot on figure 3(c) deserves a special comment. The data are for the differential cross-section at $t = 0$, therefore the corresponding theoretical curves only depend on the parametrisation of the forward scattering amplitude, and on the choice for the ϕ-meson wavefuntion. We have observed a χ^2 per point of 3.157 (resp. 1.625) for the BG (resp. LCG) wavefunction, suggesting again that the LCG wavefunction might be more appropriate to study the ϕ meson production.

- From the value of the parameter $c = 4$ GeV^{-2} obtained in our approach, we can say that the saturation scale starts to increase with momentum transfer when $t \gtrsim c^{-1} = 0.25$ GeV^2. It is interesting that this scale lies within the range of accessible data meaning that we can get insight on the dynamics of saturation by looking at the present HERA data.

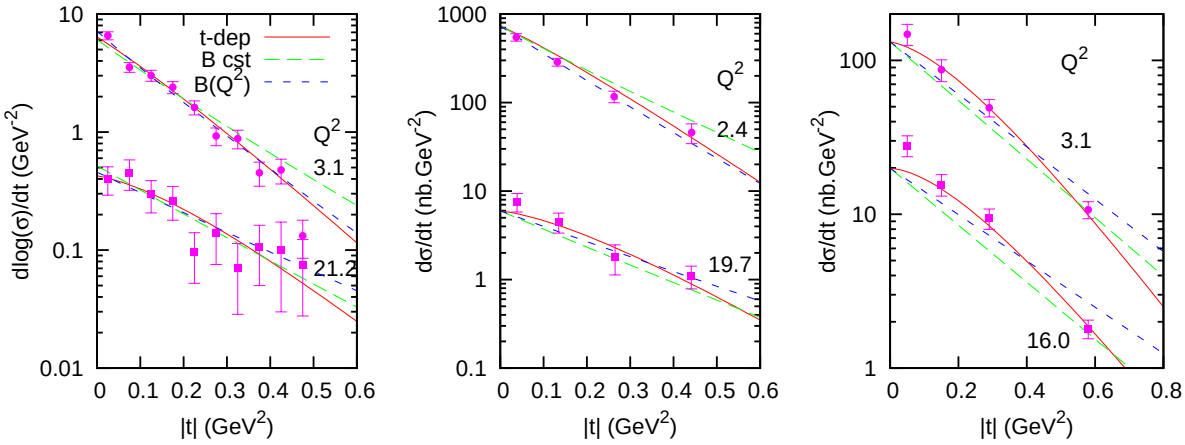

FIG. 4: Comparison of the three parametrisations for differential cross-sections. The left plot shows the ρ-meson production at Q^2=3.1 and 21.2 GeV^2, the middle one displays the ϕ meson at Q^2=2.4 and 19.7 GeV^2, and the rightmost corresponds to the J/Ψ meson at Q^2=3.1 and 16.0 GeV^2. Continuous lines: t-dependent saturation; fat-dashed lines: t-independent saturation, fixed slope; thin-dashed lines: Q^2-dependent slope.

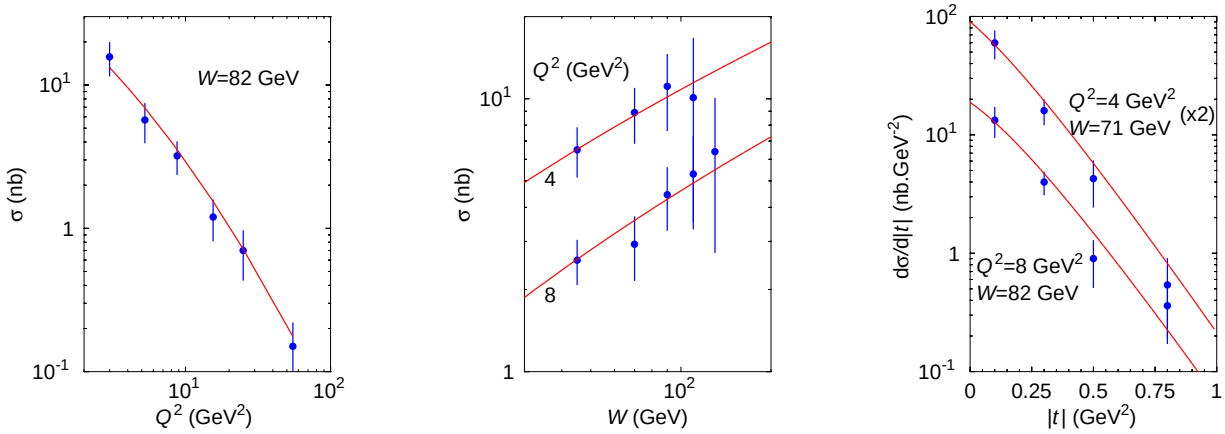

(a) $\gamma^* p \to \gamma p$ at fixed W (b) $\gamma^* p \to \gamma p$ at fixed Q^2 (c)Differential cross-section

FIG. 5: Predictions for the DVCS measurements. The data are from H1 [25].

D. Predictions for DVCS

Using the overlap function (7) in formula (6), we can predict the DVCS cross-section. Those predictions obtained with our model and the parameters determined above are presented in Figure 5. They are compared with a few available data [25] and the agreement is good. Because of the rather large error bars, these data do not alter the fit described previously, when included. Note that contrarily to diffractive vector-meson production, the dipole-model description of the DVCS data involves a wavefunction that can be computed from perturbative QED and does not require a model. The DVCS predictions of the different models presented in the previous sections differ quite a lot, at least in shape, as seen in Figure 6. We hope that forthcoming DVCS data will help to further test our predictions.

V. CONCLUSIONS AND PERSPECTIVES

Following the theoretical observation that the geometric scaling property of the BK saturation equation is valid not only for inclusive but also for diffractive exclusive processes of DIS, we have proposed an extension of the parametrisation [18] (see formula (12)) to non-forward vector-meson production. The theoretical analysis predicts a saturation scale proportional to t and a factorisation of the nonperturbative proton form factor. Hence, the geometric scaling

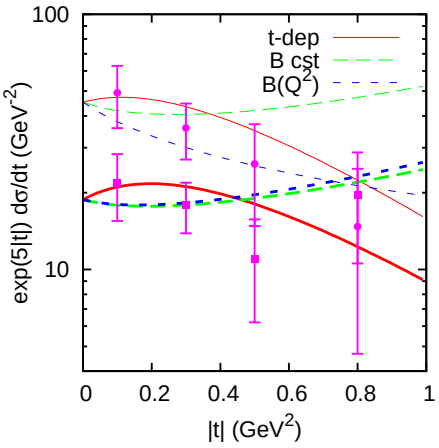

FIG. 6: Predictions of the three models studied in this paper for the DVCS diffractive cross-section. For more clarity, we have multiplied the differential cross-section by $\exp(5|t|)$. The thin lines are related to $Q^2 = 4$ GeV^2 and $W = 71$ GeV, while the thick ones are obtained with $Q^2 = 8$ GeV^2 and $W = 82$ GeV.

property, *i.e.* the $Q/Q_s(Y)$ scaling, is preserved at non-zero momentum transfer with $Q_s(t, Y) = \Omega_s(Y)f(t)$, and $f(t)$ interpolating between the soft scale at small t and $\sqrt{t}$ at higher t.

By introducing two parameters to feature the predicted behaviour of the saturation scale with t (see (10)) and the factorised non perturbative proton form factor (see (12)), we satisfactory describe the available HERA data for exclusive diffractive ρ-, ϕ- and J/Ψ-meson production. This good agreement with the data shows the consistency between QCD saturation predictions and measurements in the HERA energy range. We shall be able to further test our parametrisation when the preliminary ρ, ϕ, and DVCS data become final. Note also that the extention (12) to non-forward amplitudes could be considered for $t = 0$ saturation parametrizations other than (11).

Other successful models of exclusive processes with saturation effects have already been achieved [26, 27, 28, 29] confirming the interest of saturation physics for vector-meson production. However we would like to emphasize the specific aspect of the present work, which may open a new way to describe exclusive measurements in DIS. Indeed, within our approach, we use the momentum transfer $\mathbf{q}$ instead of the impact parameter $\mathbf{b}$ to parametrise the saturation scale. This $\mathbf{q}$-dependence is expected from p-QCD while the nonperturbative dependence in $\mathbf{q}$ is factorised, which is not the case in impact-parameter space. This is also practically convenient since the data are directly measured as a function of $t = -\mathbf{q}^2$.

Acknowledgments

We would like to thank Barbara Clerbaux, Laurent Favart, Alessia Bruni, Allen Caldwell and Miro Helbich for helping us collecting the HERA vector-meson production data. We also thank Laurent Schoeffel and Christophe Royon for insightful discussions concerning DVCS and Jean-René Cudell for useful clarifications concerning the alternative models. C.M. is supported in part by RIKEN, Brookhaven National Laboratory and the U.S. Department of Energy [DE-AC02-98CH10886]. C.M. and G.S. also thank the Galileo Galilei Institute for Theoretical Physics for hospitality and the INFN for partial support when this work was completed. G.S. is funded by the National Funds for Scientific Research (Belgium). G.S. also wants to thank the SPhT (Saclay) for hospitality when this work was started.

APPENDIX A: PHOTON AND VECTOR-MESON WAVEFUNCTIONS

For the self-consistency of the paper, let us give the expressions for the overlap functions we have used in (6) for the different processes. According to equation (1), they are the product of a wavefunction for the splitting $\gamma^* \to q\bar{q}$ and a factor accounting for the production of the final state $q\bar{q} \to \gamma^*, \gamma, V$, appropriately summed over the helicity and flavor indices.

When the final state is a photon (real or virtual), all vertices can be computed from perturbative QED at lowest order in the electromagnetic coupling. The results are

$$\begin{aligned}
\Phi_L^{\gamma^*\gamma^*}(z,\mathbf{r},Q^2) &= \sum_f e_f^2 \frac{\alpha_e N_c}{2\pi^2}\, 4Q^2 z^2(1-z)^2 K_0^2(r\bar{Q}_f), \\
\Phi_T^{\gamma^*\gamma^*}(z,\mathbf{r},Q^2) &= \sum_f e_f^2 \frac{\alpha_e N_c}{2\pi^2} \left\{[z^2+(1-z)^2]\bar{Q}_f^2 K_1^2(r\bar{Q}_f) + m_f^2 K_0^2(r\bar{Q}_f)\right\}, \\
\Phi_T^{\gamma^*\gamma}(z,\mathbf{r},Q^2) &= \sum_f e_f^2 \frac{\alpha_e N_c}{2\pi^2} \left\{[z^2+(1-z)^2]\bar{Q}_f K_1(r\bar{Q}_f) m_f K_1(rm_f) + m_f^2 K_0(r\bar{Q}_f) K_0(rm_f)\right\},
\end{aligned}$$

where e_f and m_f denote the charge and mass of the quark with flavor f and with $\bar{Q}_f^2 = z(1-z)Q^2 + m_f^2$. In practice, we sum over five flavors.

When the final state is a vector meson, the light-cone wavefunctions are usually parametrised in terms of an additional unknown vertex function for which there exists different models. The expressions to be used in (6) are then (for a vector-meson V)

$$\begin{aligned}
\Phi_L^{\gamma^* V}(z,\mathbf{r},Q^2) &= \hat{e}_f \sqrt{\frac{\alpha_e}{4\pi}} N_c\, 2Q K_0(r\bar{Q}_f) \left[M_V z(1-z)\phi_L(r,z) + \delta \frac{m_f^2 - \nabla_r^2}{M_V}\phi_L(r,z)\right], \\
\Phi_T^{\gamma^* V}(z,\mathbf{r},Q^2) &= \hat{e}_f \sqrt{\frac{\alpha_e}{4\pi}} N_c \frac{\alpha_e N_c}{2\pi^2} \left\{ m_f^2 K_0(r\bar{Q}_f)\phi_T(r,z) - [z^2+(1-z)^2]\bar{Q}_f K_1(r\bar{Q}_f)\partial_r \phi_T(r,z)\right\},
\end{aligned}$$

where the constant $\hat{e}_f$ stands for an effective charge. It is given in table III along with the quark and meson masses used. Those expressions are very similar to the ones use for photons except for the function $\phi_{L,T}$ that is related to the vertex function and depends on the model. The first choice we have investigated is the *boosted Gaussian* (BG) wavefunctions which is a simplified version of the Nemchik, Nikolaev, Predazzi and Zakharov model [15] with $\delta = 1$ and

$$\phi_{L,T} = N_{L,T} \exp\left[-\frac{m_f^2 R^2}{8z(1-z)} + \frac{m_f^2 R^2}{2} - \frac{2z(1-z)r^2}{R^2}\right].$$

The parameters R and $N_{L,T}$ are constrained by unitarity of the wavefuntion as well as by the electronic decay widths. They are given in table III.

An alternative solution is the light-cone Gauss (LCG) wavefunction [17]. For those, we take $\delta = 0$ and

$$\begin{aligned}
\phi_L &= N_L \exp\left[-r^2/(2R_L^2)\right], \\
\phi_T &= N_T\, z(1-z) \exp\left[-r^2/(2R_T^2)\right],
\end{aligned}$$

with the parameters also given in table III.

	common parameters			BG parameters			LCG parameters			
Vector-meson	M_V (GeV)	m_f (GeV)	$\hat{e}_f$	R^2 (GeV^{-2})	N_L	N_T	R_L^2 (GeV^{-2})	R_T^2 (GeV^{-2})	N_L	N_T
ρ	0.776	0.14	$1/\sqrt{2}$	12.9	0.853	0.911	10.4	21.0	1.79	4.47
ϕ	1.019	0.14	1/3	11.2	0.825	0.919	9.7	16.0	1.41	4.75
J/Ψ	3.097	1.4	2/3	2.3	0.575	0.578	3.0	6.5	0.83	1.23

TABLE III: Parameters for the vector-meson light-cone wavefunctions.

[1] A.M. Stasto, K. Golec-Biernat and J. Kwiecinski, *Phys. Rev. Lett.* **86** (2001) 596.
For a recent discussion, see F. Gelis, R. Peschanski, G. Soyez and L. Schoeffel, Phys. Lett. B **647**, 376 (2007) [arXiv:hep-ph/0610435].
[2] C. Marquet and L. Schoeffel, *Phys. Lett.* **B639** (2006) 471.
[3] A.H. Mueller, *Nucl. Phys.* **B335** (1990) 115;
N.N. Nikolaev and B.G. Zakharov, *Zeit. für. Phys.* **C49** (1991) 607.
[4] E. Iancu, K. Itakura and L. McLerran, Nucl. Phys. A **724**, 181 (2003) [arXiv:hep-ph/0212123].
[5] I. Balitsky, *Nucl. Phys.* **B463** (1996) 99; *Phys. Lett.* **B518** (2001) 235;
Yu.V. Kovchegov, *Phys. Rev.* **D60** (1999) 034008; *Phys. Rev.* **D61** (2000) 074018.
[6] S. Munier and R. Peschanski, *Phys. Rev. Lett.* **91** (2003) 232001; *Phys. Rev.* **D69** (2004) 034008; **D70** (2004) 077503.
[7] L.N. Lipatov, *Sov. J. Nucl. Phys.* **23** (1976) 338;
E.A. Kuraev, L.N. Lipatov and V.S. Fadin, *Sov. Phys. JETP* **45** (1977) 199;
I.I. Balitsky and L.N. Lipatov, *Sov. J. Nucl. Phys.* **28** (1978) 822.
[8] A. Kovner and U.A. Wiedemann, *Phys. Rev.* **D66** (2002) 051502; *Phys. Lett.* **B551** (2003) 311;
E. Ferreiro, E. Iancu, K. Itakura and L. McLerran, *Nucl. Phys.* **A710** (2002) 373.
[9] K. Golec-Biernat and A.M. Stasto, *Nucl. Phys.* **B668** (2003) 345;
E. Gotsman, M. Kozlov, E. Levin, U. Maor and E. Naftali, *Nucl. Phys.* **A742** (2004) 55.
[10] C. Marquet, R. Peschanski and G. Soyez, *Nucl. Phys.* **A756** (2005) 399.
[11] C. Marquet and G. Soyez, *Nucl. Phys.* **A760** (2005) 208.
[12] L.N. Lipatov, *Sov. Phys. JETP* **63** (1986) 904;
H. Navelet and R. Peschanski, *Nucl. Phys.* **B507** (1997) 353.
[13] G. Soyez, *Saturation QCD predictions with heavy quarks at HERA*, arXiv:0705.3672 [hep-ph].
[14] J. D. Bjorken, J. B. Kogut and D. E. Soper, Phys. Rev. D **3** (1971) 1382.
[15] J. Nemchik, N. N. Nikolaev and B. G. Zakharov, Phys. Lett. B **341** (1994) 228 [arXiv:hep-ph/9405355]; J. Nemchik, N. N. Nikolaev, E. Predazzi and B. G. Zakharov, Z. Phys. C **75** (1997) 71 [arXiv:hep-ph/9605231].
[16] L. Frankfurt, W. Koepf and M. Strikman, *Phys. Rev.* **D54** (1996) 3194.
[17] H.G. Dosch, T. Gousset, G. Kulzinger and H.J. Pirner, *Phys. Rev.* **D55** (1997) 2602;
G. Kulzinger, H.G. Dosch and H.J. Pirner, *Eur. Phys. J.* **C7** (1999) 73.
[18] E. Iancu, K. Itakura and S. Munier, *Phys. Lett.* **B590** (2004) 199.
[19] C. Marquet, *A unified description of diffractive deep inelastic scattering with saturation*, arXiv:0706.2682 [hep-ph].
[20] C. Adloff *et al.* [H1 Collaboration], Eur. Phys. J. C **13** (2000) 371 [arXiv:hep-ex/9902019].
[21] S. Chekanov *et al.* [ZEUS Collaboration], Nucl. Phys. B **718** (2005) 3 [arXiv:hep-ex/0504010].
[22] S. Chekanov *et al.* [ZEUS Collaboration], Nucl. Phys. B **695** (2004) 3 [arXiv:hep-ex/0404008].
[23] A. Aktas *et al.* [H1 Collaboration], Eur. Phys. J. C **46** (2006) 585 [arXiv:hep-ex/0510016].
[24] J. Breitweg *et al.* [ZEUS Collaboration], Eur. Phys. J. C **6** (1999) 603 [arXiv:hep-ex/9808020].
[25] A. Aktas *et al.* [H1 Collaboration], Eur. Phys. J. C **44** (2005) 1 [arXiv:hep-ex/0505061].
[26] S. Munier, A.M. Stasto and A.H. Mueller, *Nucl. Phys.* **B603** (2001) 427.
[27] H. Kowalski and D. Teaney, *Phys. Rev.* **D68** (2003) 114005.
[28] H. Kowalski, L. Motyka and G. Watt, *Phys. Rev.* **D74** (2006) 074016.
[29] J. R. Forshaw, R. Sandapen and G. Shaw, JHEP **0611** (2006) 025 [arXiv:hep-ph/0608161]; Phys. Rev. D **69** (2004) 094013 [arXiv:hep-ph/0312172].